NUCL SCI TECH (2020) 31:65
https://doi.org/10.1007/s41365-020-00780-z

# Numerical investigation of natural convection characteristics of a heat pipe-cooled passive residual heat removal system for molten salt reactors

**Cheng-Long Wang[1,2,3] · Hao Qin[1,2,3] · Da-Lin Zhang[1,2,3] · Wen-Xi Tian[1,2,3] · Guang-Hui Su[1,2,3] · Sui-Zheng Qiu[1,2,3]**

Received: 10 February 2020 / Revised: 21 April 2020 / Accepted: 27 April 2020 / Published online: 18 June 2020


**Abstract** The limited availability of studies on the natural convection heat transfer characteristics of fluoride salt has hindered progress in the design of passive residual heat removal systems (PRHRS) for molten salt reactors. This paper presents results from a numerical investigation of natural convection heat transfer characteristics of fluoride salt and heat pipes in the drain tank of a PRHRS. Simulation results are compared with experimental data, demonstrating the accuracy of the calculation methodology. Temperature distribution of fluoride salt and heat transfer characteristics are obtained and analyzed. The radial temperature of liquid fluoride salt in the drain tank shows a uniform distribution, while temperatures increase with increase in axial height from the bottom to the top of the drain tank. In addition, natural convection intensity increases with increase in height of the heat pipes in the tank. Spacing between heat pipes has no obvious effect on the natural convection heat transfer coefficient. This study will contribute to the design of passive heat removal systems for advanced nuclear reactors.

**Keywords** Molten salt reactor · Passive heat removal system · Heat pipe · Natural convection · Numerical simulation

This work was supported by the National Key R&D Program of China (No. 2019YFB1901100), the National Natural Science Foundation of China (No. 11705138), and the China National Postdoctoral Program for Innovative Talents (No. BX201600124).

Cheng-Long Wang and Hao Qin have contributed equally to this work.

✉ Cheng-Long Wang
chlwang@mail.xjtu.edu.cn

✉ Sui-Zheng Qiu
szqiu@mail.xjtu.edu.cn

1 Department of Nuclear Science and Technology, Xi'an Jiaotong University, Xi'an 710049, China

2 Shaanxi Key Laboratory of Advanced Nuclear Energy and Technology, Xi'an Jiaotong University, Xi'an 710049, China

3 State Key Laboratory of Multiphase Flow in Power Engineering, Xi'an Jiaotong University, Xi'an 710049, China

## 1 Introduction

The International Atomic Energy Agency (IAEA) Nuclear Energy Safety Report [1] highlights that in the future, more reliable, safer, and more efficient passive systems must be adopted for reactor designs to ensure that the decay heat of the reactor can be removed efficiently and passively under accident conditions [2, 3]. In recent years, heat pipes, invented at the Los Alamos National Laboratory in the 1960s, have been favored by nuclear scientists for efficient heat transfer. Their operation relies on gas–liquid two-phase flow of an internal working fluid, which transfers heat from one end of the heat pipe (evaporation section) to the other end (condensation section). Research has shown that the heat transfer capacity of heat pipes is much higher than that of metal materials. Initially, heat pipes were mainly used to solve heat dissipation problems of electronic equipment in spacecraft. With the advancement of heat pipe technology and the rapid development of the nuclear energy industry, the scope of heat pipe applications has expanded from traditional industrial sectors such as manufacturing, electronics, and energy to the design and application of large nuclear reactor systems such as space reactor optimization [4, 5], reactor containment [6, 7], small reactor core cooling [8, 9], and decommissioning after nuclear reactor accidents (e.g., Fukushima).

Preliminary neutronics and thermal hydraulic analysis shows that the temperature of fuel salt discharge during a molten salt reactor accident [10, 11] is 700–900 °C, while the effective temperature range of high-temperature heat pipes is 400–2300 °C, which completely cover the temperature range of the fuel salt [12, 13]. In addition, high-temperature heat pipes have many other advantages such as high thermal conductivity and ideal isothermality. The heat transfer mechanism of heat pipes relies on gravity or capillary pressure, which is ideal for passive operation. Finally, there is a temperature threshold for the operation of a heat pipe, which will start to work only when the temperature exceeds the threshold temperature, permitting effective temperature management. Based on these characteristics, the use of high-temperature heat pipes for removing waste heat from molten salt reactors has significant advantages [14].

A conceptual design of a heat pipe passive residual heat removal system (PRHRS) for molten salt reactors has been proposed by Wang et al. [15] and is shown in Fig. 1. The heat pipe passive waste heat removal system is mainly composed of a fuel salt drain tank, heat sink, and high-temperature heat pipe. The drain tank is connected to the core and the first circuit of the molten salt reactor through a freeze valve. One end of the high-temperature heat pipe is inserted into the drain tank, with the other end extending out of the tank. The drain tank and high-temperature heat pipe are placed in the exhaust air duct. When the reactor temperature rises above a safe limit, which may result from damage to the primary loop, loss of flow accidents, or accidental fusing of freeze valves, the temperature of the fuel salt in the pressure vessel rises rapidly, which causes the freeze valve to melt and open rapidly. The fuel salt is then gravitationally discharged into a drain tank, and the high-temperature heat pipes inserted into the drain tank begin to discharge waste heat from the accident into the atmosphere. The operation of the heat pipe type passive waste heat removal system is accomplished by three types of natural circulation (convection) couplings: (1) natural convection heat transfer between fuel salt and high-temperature heat pipes in the drain tank; (2) gas–liquid two-phase natural circulation of the working fluid in the high-temperature heat pipe; and (3) natural circulation of air in the cooling air duct. The operation of the entire passive waste heat removal system does not require any external energy input, but only depends on the natural circulation (convection) of the system. Furthermore, compared to previous designs, the system structure has been greatly simplified, effectively avoiding failure of intermediate links, and is beneficial to future modular miniaturization designs of molten salt reactors.

However, numerical and experimental investigations concerning the natural convection heat transfer characteristics of fluoride have rarely been conducted, which has seriously hindered progress in the design of heat pipe passive residual heat removal systems for molten salt reactors. In this paper, a numerical study of heat transfer characteristics of a molten salt reactor is presented, which may provide the basis for the design of passive waste heat removal systems for molten salt reactors.

The paper is arranged as follows: Sect. 1 introduces the study and provides background information about the

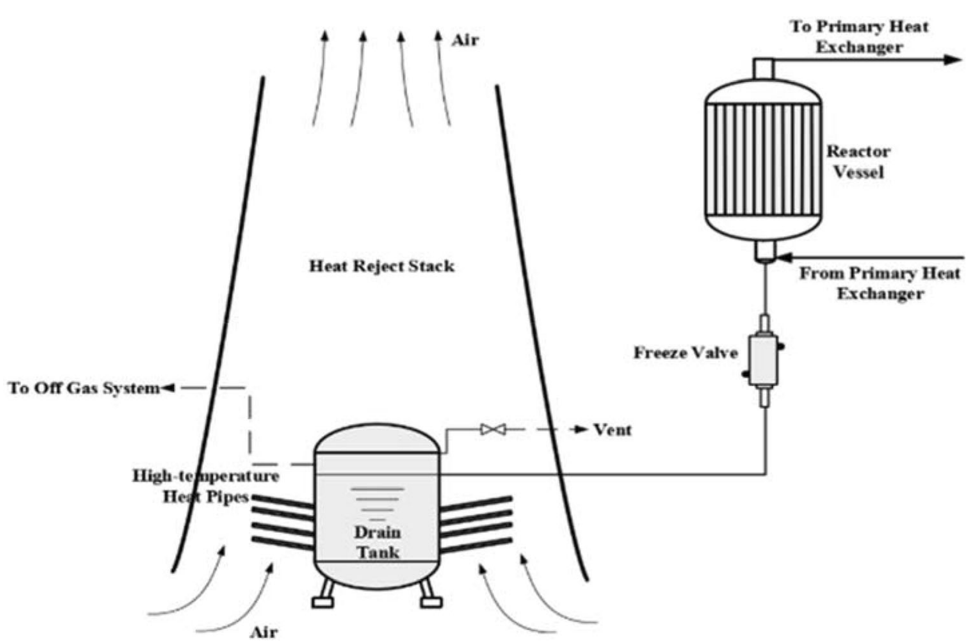


**Fig. 1** Schematic diagram of heat pipe passive waste heat removal system for molten salt reactors

application of the system; numerical methodology and models are presented in Sect. 2; validation and verification of the numerical models are given in Sect. 3; in Sect. 4, the natural convection characteristics of a heat pipe-cooled residual heat removal system are obtained and discussed, and finally, conclusions are presented in Sect. 5.

## 2 Numerical model and methodology

### 2.1 Experimental setup

An experimental system for validation of the heat pipe PRHRS was constructed and operated at Xi'an Jiaotong University (XJTU), China [16]. The system consists of an argon gas loop and a molten salt loop. The latter includes two drain tanks, two freeze pipes, and a storage tank. A schematic representation of the drain tank with inserted heat pipes is shown in Fig. 2. To simulate the fission power produced by molten salt, nine electric heating rods are inserted into the drain tank. Eight heating rods are arranged symmetrically in a circle with radius of 0.18 m, while one heating rod is located in the center. The main structural parameters are listed in Table 1.

Six drain tanks were designed and simulated in the study, which are described as follows:

1. Single heat pipe at a height of 70 mm (heat pipe A, abbreviated in Case 1).
2. Single heat pipe at a height of 200 mm (heat pipe B, abbreviated in Case 2).
3. Single heat pipe at a height of 330 mm (heat pipe C, abbreviated in Case 3).
4. With heat pipes A and C (spacing between heat pipes is 260 mm, abbreviated in Case 4).
5. With heat pipes A, B, and C (spacing between heat pipes is 130 mm, abbreviated in Case 5).

**Table 1** Model dimensions

| Parameter | Dimension (mm) |
|---|---|
| Total height | 920 |
| Length of middle section | 600 |
| Inner radius | 600 |
| Wall thickness | 10 |
| Length of each heating rod | 495 |

### 2.2 Governing equations

The continuity equation, momentum equation, and energy equation are solved using the commercial CFD software ANSYS Fluent 15.0.

Continuity equation:

$$\frac{\partial \rho}{\partial \tau} + \nabla \cdot (\rho \vec{v}) = 0, \tag{1}$$

where $\rho$ and $\vec{v}$ represent density and velocity, respectively.

Momentum equations:

$$\frac{\partial \vec{u}}{\partial \tau} + (\vec{v} \cdot \nabla)\vec{v} = \vec{f} - \frac{1}{\rho}\nabla p + \frac{\mu}{\rho}\nabla^2 \vec{v}, \tag{2}$$

where $\mu$ represents viscosity, $\vec{f}$ represents external body forces, and $\rho$ represents density.

Energy equation:

$$\rho c_p \left( \frac{\partial T}{\partial \tau} + (\vec{v} \cdot \nabla)T \right) = \lambda \nabla^2 T + \dot{\phi}, \tag{3}$$

where $T$ and $\dot{\phi}$ represent temperature and a dissipation function, respectively.

To address problems related to natural convection, the Boussinesq model is a good approximation to achieve faster convergence. In this model, density is kept constant in all solved equations, except a buoyancy term used in the momentum equation. The relationship is given as follows:

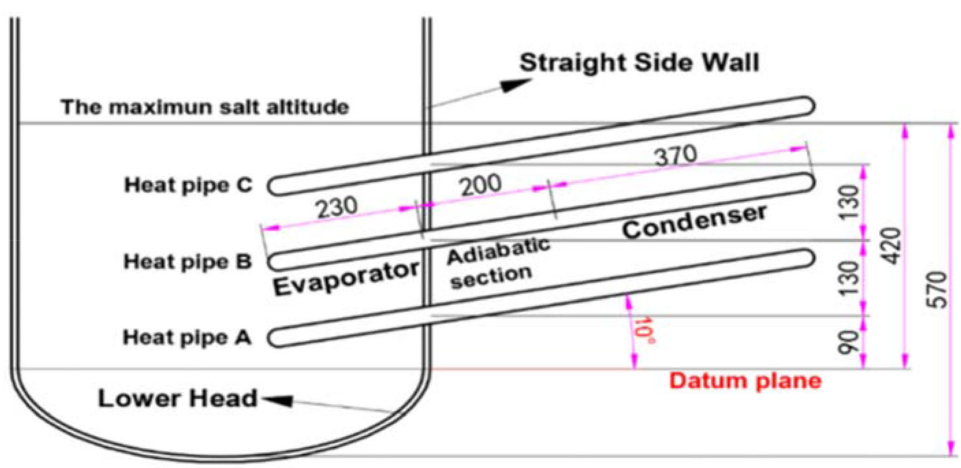


**Fig. 2** Schematic representation of the drain tank

$$(\rho - \rho_0) \gg \rho_0 \beta g \cdot \Delta T, \tag{4}$$

where $\rho_0$ is the constant density, $\beta$ represents the coefficient of thermal expansion, $g$ is the gravitational acceleration, and $\Delta T$ represents the temperature difference. The boundary conditions and thermophysical properties of the fluoride salt (FLiNaK) are listed in Tables 2 and 3.

The pressure-based solver was used in this simulation, which is recommended for incompressible flows, and a least-square cell-based method, which has a faster convergence rate and is recommended for the Boussinesq model, was used for spatial discretization. In addition, the second-order upwind scheme was selected to solve the governing equations.

### 2.3 Grid independence analysis

Four sets of meshes were adopted to obtain grid-independent results. Results become grid independent at $2 \times 10^6$ number of elements, and any further increase in the number of nodes and elements only increased computational cost and time. There is no effect on the outlet temperature, and the results become grid independent (Fig. 3a, b).

### 2.4 Data processing

The natural convection heat transfer coefficient between fluoride salts and high-temperature heat pipes can be calculated according to the following formulas:

$$\overline{Nu} = \frac{hL}{\lambda} = \frac{Q}{A\overline{\Delta T}} \times \frac{L}{\lambda}, \tag{5}$$

$$\Delta T = T_s - T_w, \tag{6}$$

$$Q = qS, \tag{7}$$

$$S = 2\pi r l, \tag{8}$$

where $T_s$ is the fluoride salt temperature, $h$ represents the heat transfer coefficient, $T_w$ is the wall temperature, $Q$ is the heat dissipation power of the side wall, $S$ is the area of the side wall, $q$ represents the heat flux of side wall, $r$ is the inner radius of the closed chamber, and $L$ represents the characteristic length of the heat pipe.

The ratio between viscosity and buoyancy forces is represented by the dimensionless Grashof number:

$$\mathrm{Gr} = gL^3 \alpha_V \Delta T / \nu^2, \tag{9}$$

where $g$ represents the gravitational acceleration, $L$ is the characteristics length of the heat pipe, $\alpha_V$ denotes the volumetric expansion coefficient, $\Delta T$ is the temperature difference [see Eq. (6)], and $\nu$ represents the kinematic viscosity.

To measure the diffusion capacity of momentum and heat, the Prandtl number is used:

$$\mathrm{Pr} = \mu c_p / \lambda, \tag{10}$$

where $c_p$ represents the specific heat capacity and $\lambda$ denotes the thermal conductivity of the working fluid. The Raleigh number is calculated using the Grashof and Prandtl numbers:

$$\mathrm{Ra} = \mathrm{Gr} \cdot \mathrm{Pr} \tag{11}$$

## 3 Model validation

To ensure reliability and accuracy of the numerical results, it is necessary to draw a comparison between experimental data and simulation results. Experimental data for single heat pipe cases (Case 1 through Case 3) were used. A comparison of static temperatures calculated through simulations with experimental data [16] was conducted, and the relative errors are shown in Table 4. Relative errors are calculated as follows:

$$e = |\mathrm{Cal.} - \mathrm{Exp.}| / \mathrm{Exp.} \times 100\%. \tag{12}$$

The calculation results are in good agreement with the experimental data, demonstrating the accuracy of the simulation methodology.

**Table 2** Boundary conditions

| Parameter | Range |
|---|---|
| Salt | FLiNaK (LiF–NaF–KF: 46.5–11.5–42 mol%) |
| Operating temperature (K) | 743–923 |
| Operating pressure (MPa) | 0.12–0.2 |
| Tank material | Type 316 stainless steel |
| Fluid level (m) | 0.42 |
| Power of heating rods (W) | 2500–4500 |
| Temperature range of heat pipes (K) | 743–833 |

**Table 3** FLiNaK thermophysical properties

| Parameter | Value |
|---|---|
| Melting point (°C) | 454 |
| Boiling point (°C) | 1570 |
| Density $\rho$ (kg m$^{-3}$) | 2729.3–0.73 $T$ |
| Viscosity $\mu$ (Pa s) | $2.487 \times 10^{-5}$ exp(4478.62/$T$) |
| Thermal conductivity $\lambda$ (W m$^{-1}$ K$^{-1}$) | $0.36 + 5.6 \times 10^{-4}$ $T$ |
| Specific heat capacity $c_p$ (J kg$^{-1}$ K$^{-1}$) | 976.78 + 1.0634 $T$ |

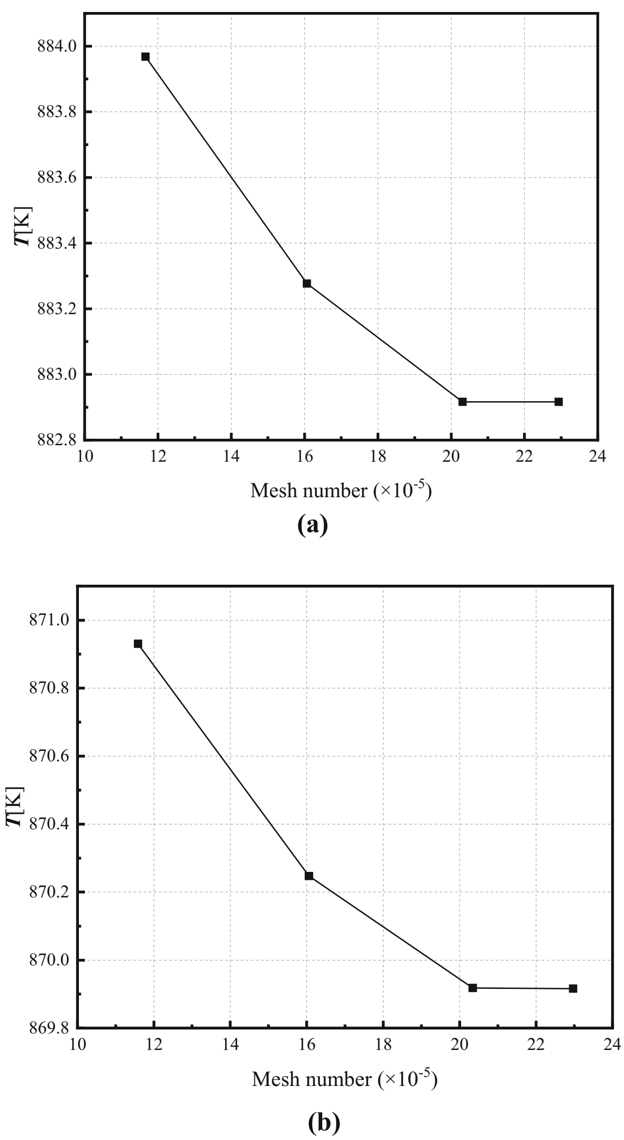


**Fig. 3** Grid independence study. **a** Case 4; **b** Case 5

## 4 Natural convection characteristics analysis of the drain tank

In this section, characteristics of natural convection heat transfer between liquid fluoride (FLiNaK) and a vertical array of heat pipes with different heights in the drain tank are analyzed and discussed.

### 4.1 Parameter sensitivity analysis

Figure 4a shows the axial temperature distribution of Case 4 at different fluoride salt temperatures and heating rod power settings. It can be seen that the axial temperature of fluoride salt gradually increases from low to high with increase in axial height, which is due to the natural circulation of fluoride in the drain tank. Figure 4b compares the temperature distribution of fluoride salts for cases where tube spacings are different, while the salt bulk temperature is kept constant. When the overall average temperature of fluoride salt in the drain tank is the same, the temperature distribution difference of fluoride salt in the tank is very small, even when the spacing of vertical tube bundles in the drain tank is different. It should be noted that the maximum temperature difference between local average temperatures of fluoride salt using two different tube spacings (0.26 m and 0.13 m) is not more than 6 K.

Figure 4 demonstrates that the axial temperature of fluoride salt varies uniformly with axial height in the straight section of the drain tank. The dimensionless temperature distribution of fluoride axial temperature and corresponding height in the straight barrel section of the drain tank is shown in Fig. 5a.

The normalized temperature of fluoride salt increases gradually with an increase in normalized height. Similar to the results for natural convection heat transfer between fluoride salt and a single heat pipe, Fig. 5a shows that regardless of the spacing of the heat pipe, the overall average temperature of fluoride salt and the power of the heating rods are different. The dimensionless distribution of the axial temperature of fluoride salt at different working conditions increases steadily from low to high, and the dimensionless average temperature of fluoride salt in the

**Table 4** Comparison between experimental data and calculation results

| *H* (mm) | Case 1 | | | Case 2 | | | Case 3 | | |
|---|---|---|---|---|---|---|---|---|---|
| | Exp. (K) | Cal. (K) | *e* (%) | Exp. (K) | Cal. (K) | *e* (%) | Exp. (K) | Cal. (K) | *e* (%) |
| 415 | 879.25 | 883.32 | 0.46 | 874.28 | 880.23 | 0.68 | 876.29 | 882.12 | 0.67 |
| 285 | 871.66 | 869.25 | − 0.28 | 865.85 | 863.15 | − 0.31 | 865.68 | 866.94 | 0.15 |
| 155 | 861.09 | 858.74 | − 0.27 | 853.87 | 858.25 | 0.51 | 857.16 | 863.11 | 0.69 |
| 25 | 845.92 | 848.64 | 0.32 | 842.82 | 837.15 | − 0.67 | 847.77 | 843.85 | − 0.46 |
| − 40 | 842.88 | 845.15 | 0.27 | 840.92 | 838.15 | − 0.33 | 845.33 | 841.25 | − 0.48 |

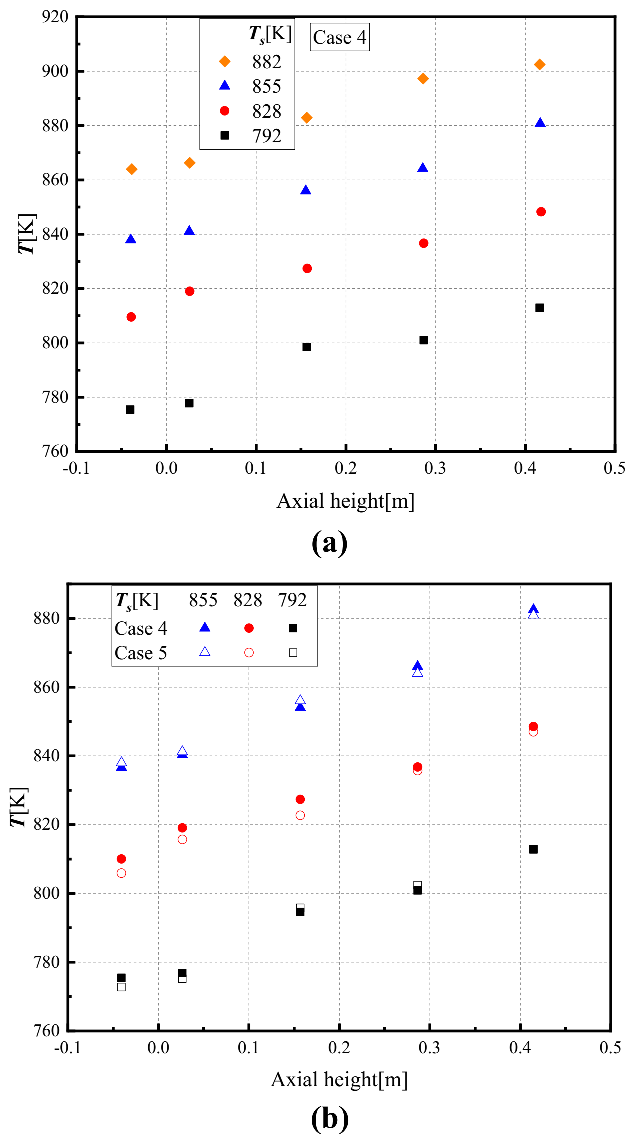


**Fig. 4** Temperature distribution characteristics. **a** Molten salt temperature variations with axial height; **b** variation of salt temperatures with different heat pipe spacing

straight section of drain tank shows the following linear relationship:

$$T_s/T_b = 0.04975 \cdot H/H_{max} + 0.98011, \tag{13}$$

where the $T_b$ is the bulk temperature of the molten salt.

Figure 5b shows the temperature difference variation of fluoride salt relative to the average temperature of fluoride salt inside the tank, which was measured with the help of measuring points in the drain tank.

Figure 5c shows the temperature difference variation of fluoride salt relative to the average power setting of the heat pipes. It is evident that the temperature difference of fluoride salt remains essentially unchanged under all working conditions.

## 4.2 Analysis of heat transfer characteristics

On the basis of the simulation results, the natural convection process between fluoride salt and heat pipes was further analyzed. The natural convection heat transfer coefficient between liquid fluoride (FLiNaK) and two differently spaced vertical heat pipe bundles (Case 4 and Case 5) is shown in Fig. 6a. Natural convection heat transfer coefficients for fluoride salt and the vertical tube bundles remain similar for both cases, with no obvious difference between heat transfer coefficients for different heat pipe spacings.

With an increase in fluoride salt temperature, natural convection becomes increasingly intense, leading to increases in the natural convection heat transfer coefficient and convection intensity. When the overall average temperature of fluoride salt in drain tank increases from 790 to 850 K, the resulting value for the natural convection heat transfer coefficient increases from 620 to 710 W m$^{-2}$ K$^{-1}$. In Fig. 6a, values for the natural convection heat transfer coefficient of a single heat pipe are shown for comparison with the vertical heat pipe arrays. For a single heat pipe, the overall average temperature of fluoride salt increases from 779 to 880 K, and as a result, the natural convection coefficient increases from 720 to 790 W m$^{-2}$ K$^{-1}$. It is clear that the natural convection heat transfer coefficient of fluoride salt using vertical tube bundles is significantly (15%) lower compared to a single heat pipe setup.

Figure 6b shows the variation of the average heat dissipation power of heat pipes relative to the temperature difference between the fluoride salt and the average wall

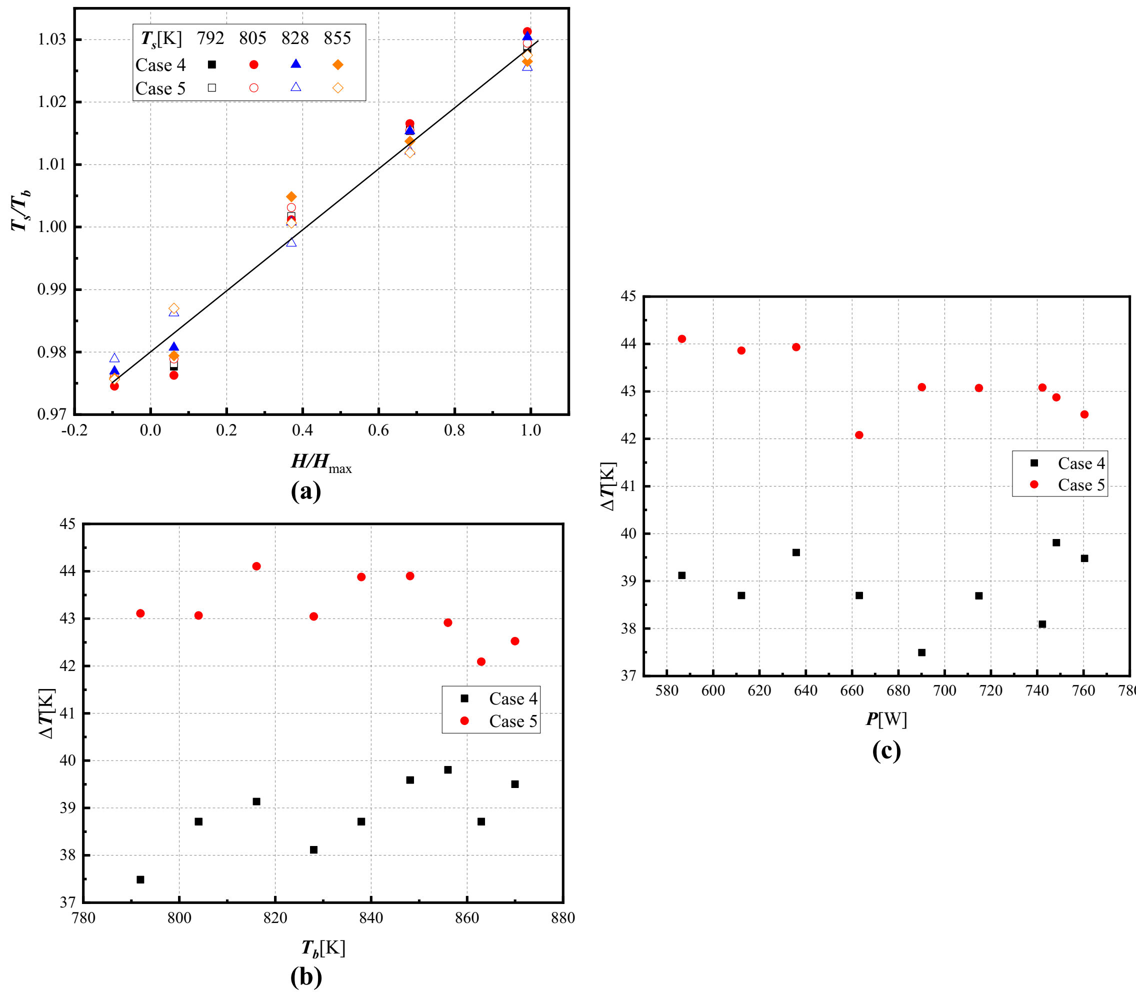


**Fig. 5** Temperature difference analysis. **a** Dimensionless axial temperature distribution of fluoride salt; **b** variations of the temperature difference of fluoride salt relative to the average temperature of fluoride salt; **c** variations of the temperature difference of fluoride salt relative to the average power setting of the heat pipes

temperature of the heat pipe under different conditions. It is evident that the average heat dissipation power between fluoride salt and heat pipes is lower for the vertical arrays of heat pipes compared with that of a single heat pipe. Although the average power of the heating rods for the vertical arrays of heat pipes is higher, the heat dissipation power for a single heat pipe is 100 W higher than that for the vertical arrays of heat pipes. The decrease in average heat dissipation power and convective heat transfer coefficient for the vertical arrays of heat pipes indicates that the natural convection intensity of fluoride salt is weakened as shown in Fig. 6b. There may be two reasons for this behavior: (1) the arrangement of the vertical bundles of heat pipes interferes with the natural convection flow of the fluoride salt, resulting in a decrease of the average convection heat transfer capacity between fluoride salt and each heat pipe. Similar experiments with water as working fluid show that the wake generated by water flowing through the lower tube affects the flow of water outside the upper tube, hindering heat transfer and reducing heat dissipation power [17]; (2) flow constriction limits the heat transfer intensity. In a closed and narrow drain tank, natural convection between the tube bundle and fluoride salt cannot fully develop, limiting flow and heat transfer [18].

Figure 6c shows average Nusselt numbers (Nu) representing natural convection heat transfer between fluoride salt and vertical tube bundles relative to Rayleigh numbers for different tube spacings. It is evident that Nu increases with increase in Ra numbers. Due to a weakening of the overall natural convection intensity, average Nusselt numbers vary from 23 to 25, which is significantly smaller than for a single heat pipe.

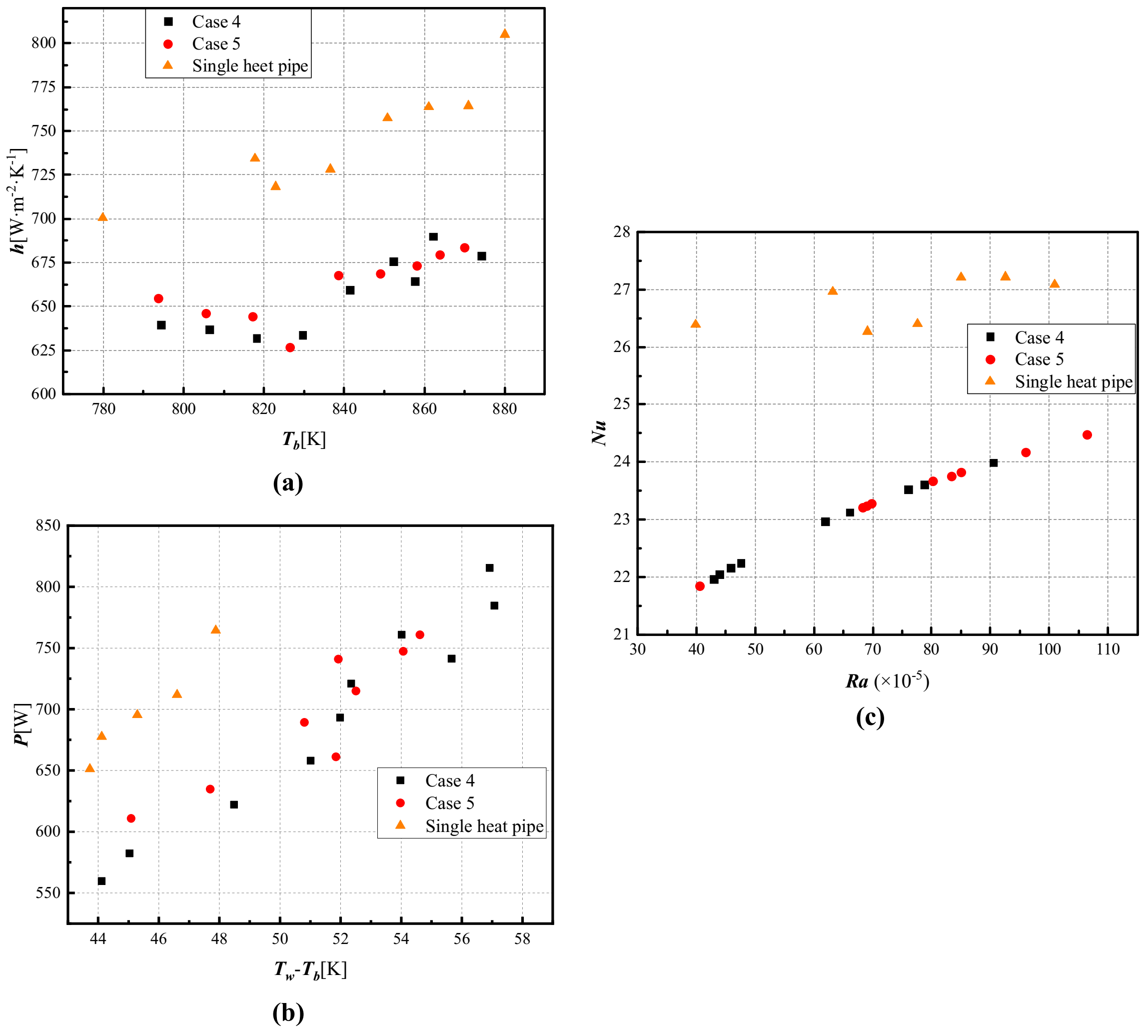


**Fig. 6** Heat transfer characteristics. **a** Comparison of heat transfer coefficients for a single heat pipe versus vertical arrays of heat pipes; **b** average heat dissipation power (***P***) of vertical arrays of heat pipes compared with a single heat pipe; **c** relationship between Nu and Ra numbers

## 5 Conclusion

Numerical investigations of natural convection heat transfer characteristics of fluoride salt in a drain tank were conducted in this study. The simulation methodology was validated by comparing the calculation results with experimental data. Main conclusions are summarized as follows:

1. The radial temperature of liquid fluoride salt in the drain tank shows a uniform distribution; however, the salt temperature increases with increase in axial height from bottom to top.
2. The average temperature of fluoride salt and the average heat dissipation power of the heat pipe have no obvious influence on temperature differences within the tank.
3. The natural convection heat transfer coefficient increases with increase in temperature of the fluoride salt. The natural convection intensity increases with an increase in the height of the heat pipe in the tank. The spacing between heat pipes shows no obvious effect on the natural convection heat transfer coefficient.

Based on these conclusions, several suggestions for the design of a PRHRS can be made: (1) the vertical position of heat pipes should be reasonably high to enhance natural convection heat transfer; and (2) to increase heat transfer, the number of heat pipes should be increased considering that heat pipe spacing has a negligible effect on heat transfer.

## References


1. IAEA, Nuclear Safety Review for 2018, Vienna (2019)

2. M. Lin, M. Cheng, Z. Dai, Feasibility of an innovative long-life molten chloride-cooled reactor. Nucl. Sci. Tech. **31**, 33 (2020). https://doi.org/10.1007/s41365-020-0751-7
3. X. Jiang, H. Lu, Y. Chen et al., Numerical and experimental investigation of a new conceptual fluoride salt freeze valve for thorium-based molten salt reactor. Nucl. Sci. Tech. **31**, 16 (2020). https://doi.org/10.1007/s41365-020-0729-5
4. W. Zhang, D. Zhang, W. Tian et al., Thermal-hydraulic analysis of the improved TOPAZ-II power system using a heat pipe radiator. Nucl. Eng. Des. **307**, 218–233 (2016). https://doi.org/10.1016/j.nucengdes.2016.07.020
5. W. Zhang, C. Wang, R. Chen et al., Preliminary design and thermal analysis of a liquid metal heat pipe radiator for TOPAZ-II power system. Ann. Nucl. Energy **97**, 208–220 (2016). https://doi.org/10.1016/j.anucene.2016.07.007
6. Y. Yuan, J. Shan, B. Zhang et al., Accident analysis of heat pipe cooled and AMTEC conversion space reactor system. Ann. Nucl. Energy **94**, 706–715 (2016). https://doi.org/10.1016/j.anucene.2016.04.017
7. M.M. Razzaque, On application of heat pipes for passive shutdown heat removal in advanced liquid metal and gas-cooled reactor designs. Ann. Nucl. Energy **17**, 139–142 (1990). https://doi.org/10.1016/0306-4549(90)90091-Q
8. S.B. Seo, I.G. Kim, K.M. Kim et al., Risk mitigation strategy by passive IN-core cooling system for advanced nuclear reactors. Ann. Nucl. Energy **111**, 554–567 (2018). https://doi.org/10.1016/j.anucene.2017.09.030
9. K.M. Kim, I.C. Bang, Heat transfer characteristics and operation limit of pressurized hybrid heat pipe for small modular reactors. Appl. Therm. Eng. **112**, 560–571 (2017). https://doi.org/10.1016/j.applthermaleng.2016.10.077
10. H. Qin, C. Wang, S. Qiu et al., Study of tritium transport characteristics in a transportable fluoride-salt-cooled high-temperature reactor. Int. J. Energy Res. **42**, 1536–1550 (2018). https://doi.org/10.1002/er.3944
11. H. Qin, C. Wang, D. Zhang et al., Transient analysis of tritium transport characteristics in fluoride-salt-cooled high-temperature reactor. Prog. Nucl. Energy **117**, 103064 (2019). https://doi.org/10.1016/j.pnucene.2019.103064
12. K. Ma, C. Yu, X. Cai et al., Transmutation of I-129 in a single-fluid double-zone thorium molten salt reactor. Nucl. Sci. Tech. **31**, 10 (2020). https://doi.org/10.1007/s41365-019-0720-1
13. X. Li, D. Cui, Y. Ma et al., Influence of U-235 enrichment on the moderator temperature coefficient of reactivity in a graphite-moderated molten salt reactor. Nucl. Sci. Tech. **30**, 166 (2019). https://doi.org/10.1007/s41365-019-0694-z
14. J. Tournier, M.S. El-Genk, Startup of a horizontal lithium–molybdenum heat pipe from a frozen state. Int. J. Heat Mass Transf. **46**, 671–685 (2003). https://doi.org/10.1016/S0017-9310(02)00324-1
15. C. Wang, D. Zhang, S. Qiu et al., Study on the characteristics of the sodium heat pipe in passive residual heat removal system of molten salt reactor. Nucl. Eng. Des. **265**, 691–700 (2013). https://doi.org/10.1016/j.nucengdes.2013.09.023
16. M. Liu, D. Zhang, C. Wang et al., Experimental study on the heat transfer characteristics of fluoride salt in the new conceptual passive heat removal system of molten salt reactor. Int. J. Energy Res. **42**, 1635–1648 (2018). https://doi.org/10.1002/er.3959
17. T. Persoons, I.M.O. Gorman, D.B. Donoghue et al., Natural convection heat transfer and fluid dynamics for a pair of vertically aligned isothermal horizontal cylinders. Int. J. Heat Mass Transf. **54**, 5163–5172 (2011). https://doi.org/10.1016/j.ijheatmasstransfer.2011.08.033
18. R. Chouikh, A. Guizani, A. El Cafsi et al., Experimental study of the natural convection flow around an array of heated horizontal cylinders. Renew. Energy **21**, 65–78 (2000). https://doi.org/10.1016/S0960-1481(99)00120-2